crystals

MDPI

SUPPLEMENTARY MATERIALS

The Jahn-Teller Distortion at High Pressure: The Case of Copper Difluoride

Dominik Kurzydłowski

1. Ambient-Pressure X-Ray Diffraction

The crystallinity and purity of CuF_2 was investigated with the use of powder X-ray diffraction. Figure S1 shows a powder diffractogram obtained with the X'Pert Pro diffractometer (Panalytical, Almeo, Holand) using a cobalt X-ray source ($I(CoK_{\alpha 1})/I(CoK_{\alpha 2}) = 2$; angle range from 10° to 60°; acquisition time 5 h). As can be clearly seen the sample is manly composed of CuF_2 with only a minor contamination (less than 7 vol%) identified as hydrated copper difluoride ($CuF_2{\cdot}2H_2O$).

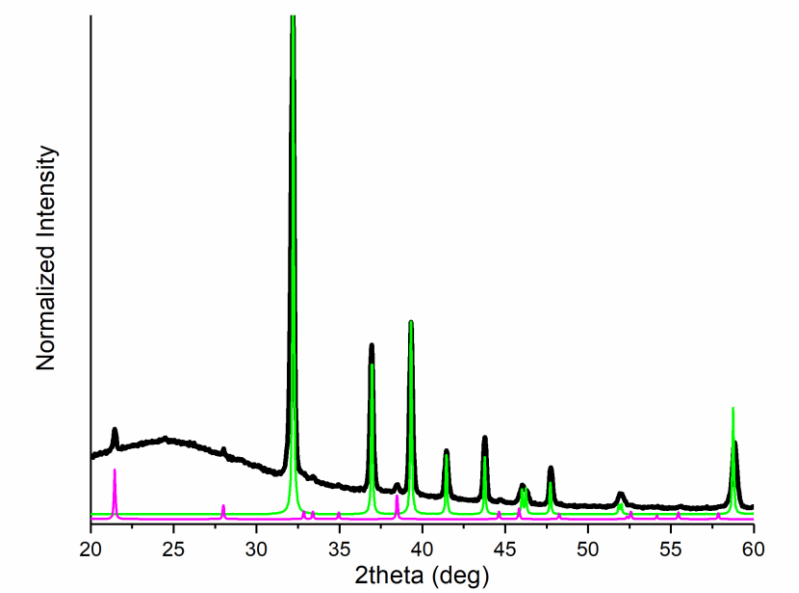

Figure S1 The experimental powder X-ray diffraction pattern of a sample of CuF_2 (black line) together with patterns simulated for the CuF_2 crystal (green) and $CuF_2{\cdot}2H_2O$ (magenta).

2. Deconvolution of the Raman Spectrum of CuF_2 at 19.6 GPa

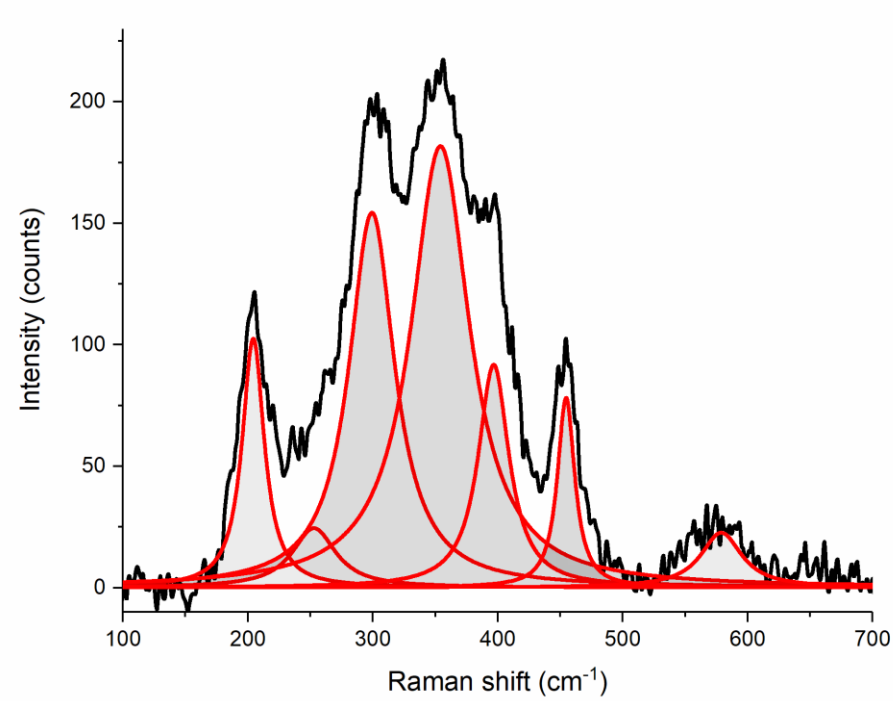

Figure S2 The experimental Raman spectrum of CuF_2 (black line) together with the deconvolution into Lorentzian profiles (red lines).

3. Inter-Sheet vs. Intra-Sheet Compressibility of *P2₁/c* and *Pbca*

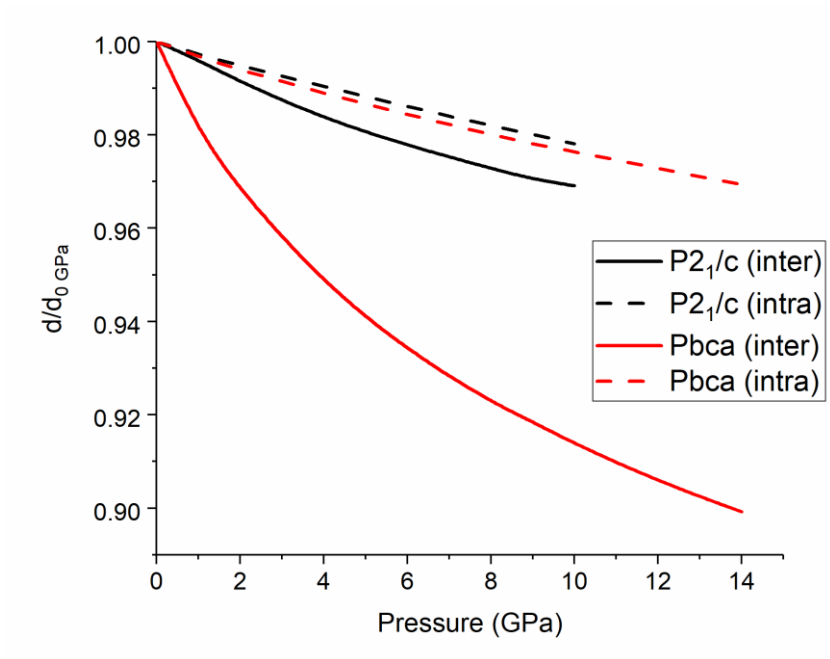

Figure S3 Comparison of the compressibility of inter-sheet (full lines) and intra-sheet (dashed lines) Ag-Ag distances in *P2₁/c* (black) and *Pbca* (red).

Note that from Figure S3 it is evident that *Pbca* exhibits much softer behavior of the inter-sheet contacts compared with *P2₁/c*, which is in line with its smaller bulk modulus.

4. Comparison of Raman-Active Modes of ZnF_2 and CuF_2

Zinc difluoride (ZnF_2) adopts the undistorted rutile structure (*P4₂/mnm*) which exhibits four Raman-active modes: B_{1g}, E_g, A_{1g}, and B_{2g} (Table S1). Upon the symmetry lowering to the *P2₁/c* space group (adopted by CuF_2) the E_g mode splits into two non-degenerate modes (B_g and A_g), while the silent A_{2g} mode transforms to a Raman-active B_g mode (Table S1). As a result CuF_2 exhibits six Raman-active modes.

Table S1. Comparison of Γ-point Raman-active modes of ZnF_2 and CuF_2. Experimental frequencies obtained at ambient pressure (ω_0) are given in cm^{-1}.

ZnF_2			CuF_2	
ω_0[1]	Symmetry		Symmetry	ω_0
69	B_{1g}	→	A_g	n.d.
240	E_g	→	B_g	221
		→	A_g	254
n.d.[2]	A_{2g}[2]	→	B_g	293
347	A_{1g}	→	A_g	355
523	B_{2g}	→	B_g	566

[1] Data from ref [24]; [2] silent mode.

The largest differences between frequency of symmetry-related modes is found for the highest energy B_g mode of CuF_2 which is shifted up by 43 cm^{-1} compared to the B_{2g} mode of ZnF_2. One might speculate that this difference is a result of the JT distortion of the Cu^{2+} octahedron.

The comparison of the two modes indicates that the both involve stretching of a pair of Zn-F/Cu-F bonds (Figure S4). For the CuF_2 this is a pair of equatorial bonds which are JT-shortened compared

to analogous bonds found in ZnF_2 by about 0.14 Å at ambient pressure. Thus, as expected, the higher frequency of the B_g mode stems from the distortion induced by the JT effect.

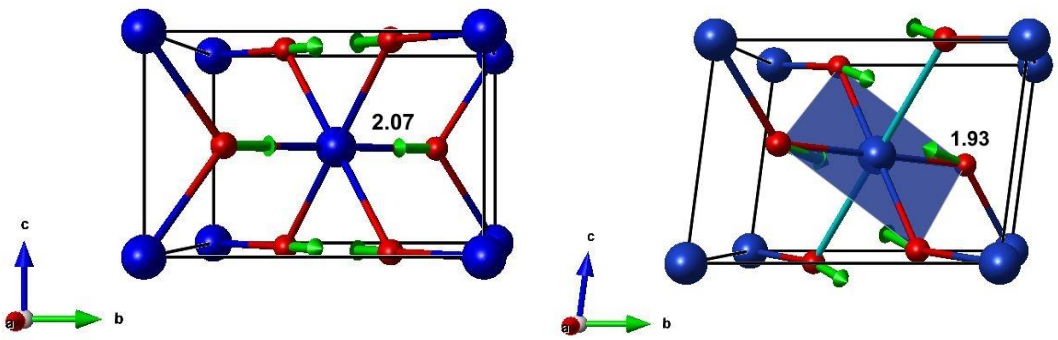

Figure S4 Comparison of the eigenvectors of the B_{2g} mode of ZnF_2 (**left**), and the symmetry-related B_g mode of CuF_2 (**right**). The calculated distances of the Zn-F/Cu-F bonds which undergo stretching along these modes are given in Å.

Comparison of the calculated pressure evolution of the abovementioned bonds indicates that upon compression the difference between these bonds decreases to about 0.11 Å at 9 GPa (Figure S5). This is in line with the reduction of the JT effect in the $P2_1/c$ structure of CuF_2 at higher pressure (see Figure 7a).

This reduction should lead to a decrease in the difference between the frequencies of the B_g and B_{2g} modes. Unfortunately the pressure dependence of the B_{2g} mode of ZnF_2 has not been established experimentally, therefore, we compared those calculated theoretically (Figure S5). As can be seen the difference becomes smaller upon compression (40 cm^{-1} at 0 GPa to 27 cm^{-1} at 9 GPa).

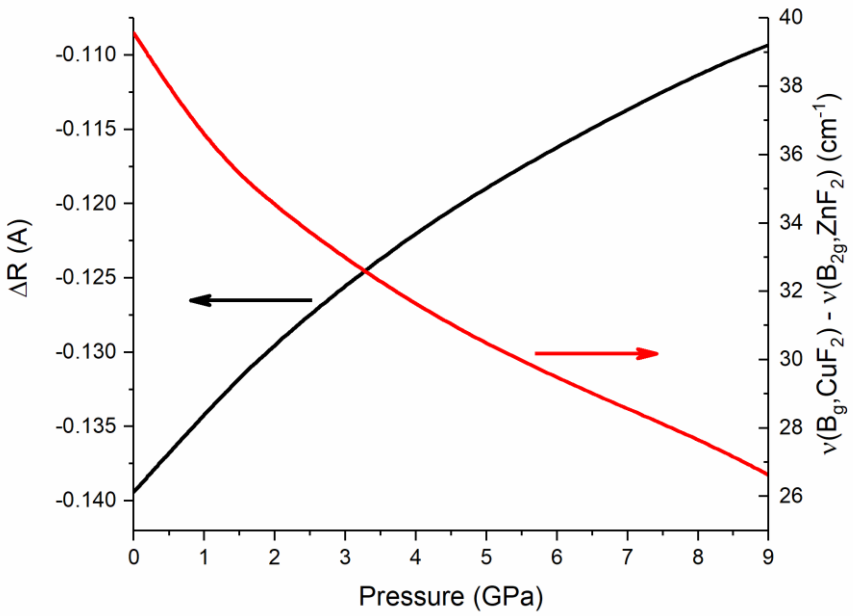

Figure S5 Calculated pressure evolution of the difference between the Zn-F/Cu-F bonds highlighted in Figure S4 (black line) together with the predicted differences in the frequencies of the highest B_g mode of CuF_2 and the B_{2g} mode of ZnF_2 (red line).

5. Spin Density in *Pbca* at 30 GPa and *Pnma* at 100 GPa

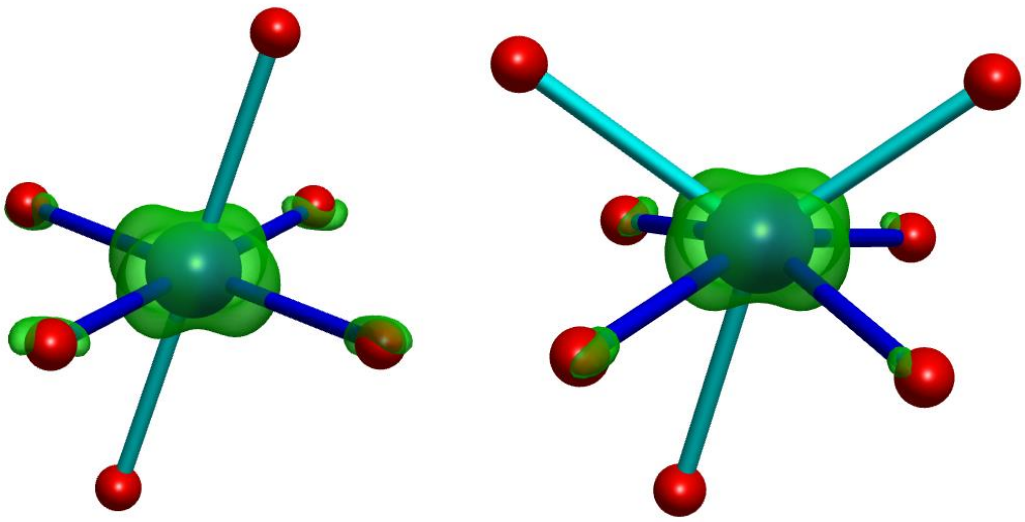

Figure S6 Comparison of the spin-density (green surface) calculated for *Pbca* at 30 GPa (**left**) and *Pnma* at 100 GPa (**right**). The isosurface is drawn at 0.2 $Å^{-3}$.

6. Relative Enthalpies of the Cotunnite and HP-PdF_2 Phases of ZnF_2

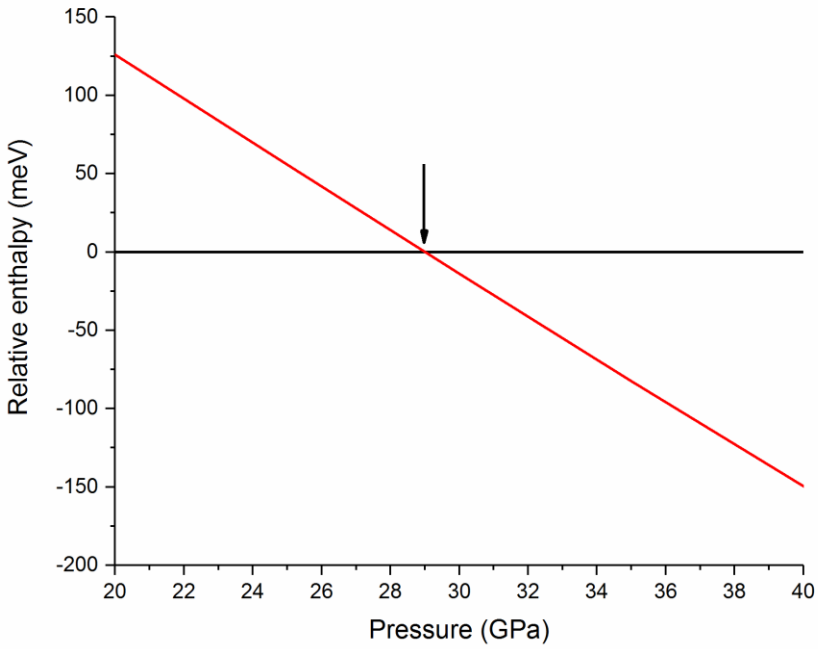

Figure S7 The pressure dependence of the relative enthalpy of the cotunnite phase of ZnF_2 (red line) referenced to that of the HP-PdF_2 phase (black line). The arrow marks a predicted phase transition at 29 GPa.